Microbial Cell Factories

RESEARCH

Open Access

Biodegradation of *p*-nitrophenol by *Rhodococcus* sp. 21391 unveils a two-component *p*-nitrophenol monooxygenase with broad substrate specificity

Jian Yang[1,2*†], Shanshan Lin[2,3†], Wei Li[2,3], Xianjie Wang[2,3] and Ru Li[2,3*]

Abstract

Background Bioremediation relying on highly efficient degrading bacteria constitutes a promising and sustainable avenue for controlling and reducing nitrophenol contamination in the environment. A thorough understanding of the bacterial degradation mechanism of nitrophenol is of paramount importance for supporting the development of efficient microbial remediation technology.

Results In this study, a new bacterium, *Rhodococcus* sp. 21391, endowed with superior *p*-nitrophenol (PNP) degradation ability was obtained. Genomic and comparative proteomic analyses revealed that it utilizes the 1,2,4-benzenetriol (BT) pathway for PNP degradation. The catalytic properties of the two-component *p*-nitrophenol monooxygenase RsNcpAB from the strain were investigated in vitro. The enzyme exhibited a broad substrate selectivity, catalyzing the oxidation of various nitrophenols and halogenated phenols, with significant potential for further research and development. Additionally, the crystal structure of the oxidative component of *p*-nitrophenol monooxygenase, RsNcpA, was determined. Structural analysis and site-directed mutagenesis revealed that residues Arg100 and His293 in the active site play a crucial role in enzyme catalysis, and a catalytic mechanism model was subsequently proposed.

Conclusions This study reports a high-performance nitrophenol-degrading bacterium and enzyme, and reveals their mechanisms at the molecular level. These findings increase the understanding of the bacterial degradation of nitrophenol, thereby providing a crucial foundation for the development of efficient bioremediation technologies.

Keywords Nitrophenol biodegradation, Comparative proteome, *p*-nitrophenol monooxygenase, Substrate specificity

[†]Jian Yang and Shanshan Lin contributed equally to this work.

*Correspondence:
Jian Yang
yangjian@dgut.edu.cn
Ru Li
honey_liru@163.com
Full list of author information is available at the end of the article

Graphical Abstract

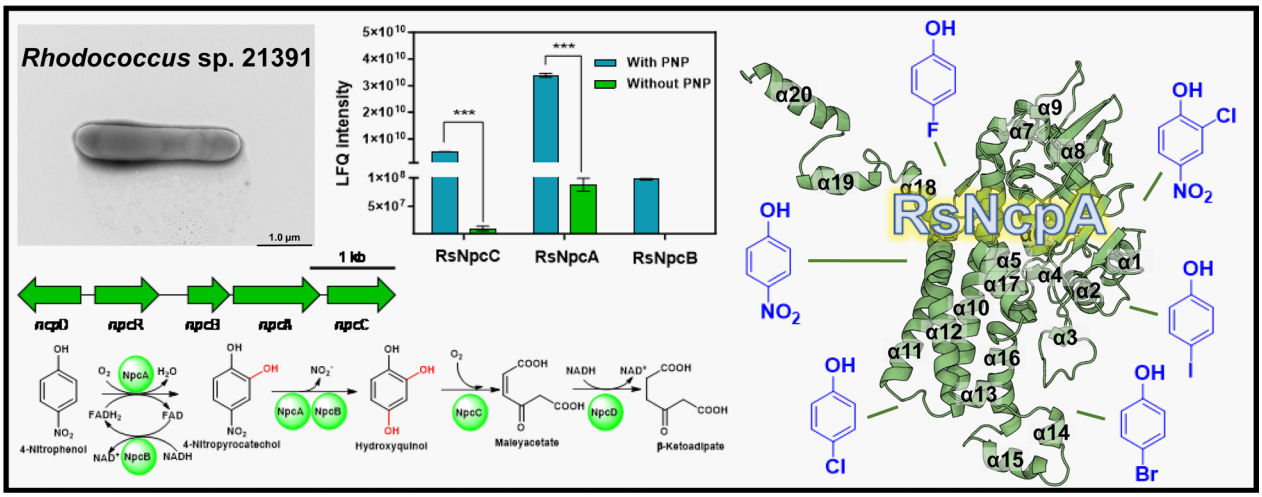

Introduction

Nitrophenols constitute a group of organic compounds of significant environmental concern. These substances can enter the environment via a plethora of anthropogenic activities including industrial processing, agricultural run-off, and improper waste management [1, 2]. Nitrophenols have been listed as priority controlled pollutants in many countries because of their high level of toxicity, oncogenicity, and biological accumulation [3–5]. Upon the entry of nitrophenols into the bloodstream, they can transform hemoglobin to methemoglobin, thereby inducing liver impairment, anemia, dyspnea and other symptoms [6, 7]. The frequent occurrence of nitrophenols in the environment calls for the development of efficient methods for controlling nitrophenol pollution.

Several remediation strategies involving physical, chemical, and biological approaches have been devised [1, 8, 9]. Among these, the microbial remediation of nitrophenols harbors great potential on account of its cost-effectiveness, environmental friendliness, adaptability, and in situ application capabilities. Microbes have evolved metabolic pathways to utilize nitrophenols, transforming them into less harmful substances [10–12]. This process can be applied in situ to foster the sustainable self-cleaning capacity of the environment under mild conditions, diminishing the need for extreme temperatures or pressures. Furthermore, microbial remediation does not generate large quantities of toxic by-products and has a lower ecosystem impact [13].

Genomic investigations have identified specific genes encoding enzymes involved in nitrophenol biodegradation. Two distinct nitrophenol catabolic pathways have been elaborately elucidated. Nitrophenol is degraded via the 1,2,4-benzenetriol (BT) pathway in Gram-positive bacteria, with BT 1,2-dioxygenase catalyzing ring cleavage [14–16]. Along this pathway, nitrophenols such as *p*-nitrophenol (PNP) are converted to *p*-nitrocatechol and BT by two-component PNP monooxygenases. Subsequently, BT undergoes ring cleavage to enter the central metabolism. In contrast, in Gram-negative strains, nitrophenol is degraded through the hydroquinone (HQ) pathway [12, 17]. These strains catabolize nitrophenol with HQ as the ring-cleavage intermediate, and its complete degradation is catalyzed by HQ dioxygenase. The initial step of both the BT and HQ pathways is catalyzed by *p*-nitrophenol monooxygenases, whose catalytic site selectivity results in the formation of distinct nitrophenol metabolic pathways. The catalytic selectivity of the two classes of *p*-nitrophenol monooxygenases is important for understanding the principle behind the bacterial degradation of nitrophenols. Nevertheless, in-depth investigation into their molecular mechanisms is limited.

This investigation reports the discovery and mechanistic characterization of a two-component monooxygenase (RsNcpAB) exhibiting unprecedented catalytic versatility from a novel *Rhodococcus* strain isolated from mangrove ecosystems. Through multi-omics approaches integrating comparative genomics, proteome profiling, and enzymatic assays, we systematically mapped the complete PNP mineralization pathway while identifying RsNcpAB as its gatekeeping catalyst. Crucially, structural and functional analyses revealed this flavin-dependent monooxygenase possesses an unusually broad substrate spectrum—capable of oxygenating diverse aromatic

compounds through its unique substrate recognition mechanism. X-ray crystallography combined with targeted mutagenesis unveiled an architecturally distinct catalytic pocket featuring flexible substrate-accommodating loops, providing the structural basis for substrate promiscuity in this enzyme. This mechanistic breakthrough not only redefines our understanding of microbial nitrophenol metabolism but establishes RsNcpAB as a prime engineering template for developing multifunctional biocatalysts addressing mixed contaminant scenarios in environmental biotechnology.

Material and methods

Strain isolation and identification

Approximately 1 g of mangrove soil (Sanya, China) was suspended in 100 mL of mineral salts medium (MSM) with shaking at 100 rpm at 25 °C for 1 h. Aliquots of the diluted suspension were spread onto the agar plates containing 300 μM PNP as the sole carbon source. The plates were incubated for 5 days at 25 °C, and distinct colonies were selected and subjected to purification to obtain pure cultures. The degrading ability of the purified strains was measured by analyzing the concentration of PNP at regular intervals after inoculation into liquid MSM medium with 300 μM PNP. Morphological characteristic analysis and 16S rRNA sequencing were employed for species identification. The neighbor-joining phylogenetic tree was constructed using MEGA7 with 1000 bootstrap values based on the 16S rRNA gene sequences of the strains and their closest species [18].

PNP degradation ability analysis of the bacterial strain

The obtained PNP-degrading bacterium was inoculated into Tryptic Soy Broth medium and shaken at 25 °C and 150 rpm until the optical density at 600 nm (OD600) reached 1.0. The bacterial cells were collected (4 °C, 5000×*g* centrifugation) and washed three times with 50 mM phosphate buffer (pH 7.2). The washed cells were inoculated into 200 mL of MSM containing 300 μM PNP, and the cell density was adjusted to OD600 = 0.1. The mixture was incubated at 25 °C with shaking at 100 rpm, and samples were taken each 2 h to determine the cell density and PNP content. The content of PNP was determined by high-performance liquid chromatography (Agilent 1260, Agilent Technologies, Palo Alto, CA, USA) using a Zorbax SB-C18ODS column (4.6 × 150 mm, 5 μm, Agilent Technologies), with a diode array detector and a detection wavelength of 320 nm. The mobile phase was 0.1% (*v*/*v*) acetic acid containing a 5%–100% methanol linear gradient flowing at 1 ml/min, 30 °C. Each group of experiments was repeated at least three times.

Genome sequencing and annotation

Whole-genome sequencing and annotation of *Rhodococcus* sp. 21391 were conducted by Sangon Biotech (Shanghai, China). Briefly, the strain was cultured to exponential phase and the cells were collected using centrifugation at 5000×*g* for 5 min, and the bacterial total DNA was extracted. Genome sequencing was then carried out using the third-generation PacBio platform (Huada Gene Co., Ltd., Shenzhen, China). Software SMRT v. v2.2.0 and GATK v. v1.6–13 were used to assemble the continuous contigs, and credible complete sequences were generated after single-base correction and loop judgment based on the obtained contigs. The genome was annotated using the prokaryotic genome annotation pipeline of the National Center for Biotechnological Information. The complete chromosome and plasmids sequences of *Rhodococcus* sp. 21391 has been deposited in GenBank database with accession numbers CP063781-CP063784.

Comparative proteomic analysis

Cells of *Rhodococcus* sp. 21391 were grown in Tryptic Soy Broth at 30 °C and 180 rpm to an OD_{600} of 1.0. Harvested cells were washed three times in 50 mM phosphate buffer (pH 7.5) and resuspended in MSM containing 300 μM PNP (experimental cultures) or MSM without PNP (control cultures). After 6 h of induction at 25 °C and 100 rpm, 2 mL aliquots were pelleted at 5000×*g* (4 °C), lysed via sonication (10 min on ice), and boiled for 15 min. Clarified supernatants were collected after centrifugation (12,000×*g*, 30 min), and protein concentrations were normalized to 2 μg/μL using the Bradford assay [19]. Proteins (100 μg) were digested with trypsin (1 μg, 4 h; followed by 1 μg, 12 h) at 37 °C. Resulting peptides were analyzed by nano-liquid chromatography-tandem mass spectrometry (nanoLC-MS/MS) on a C18 column using a gradient of 0.1% formic acid and acetonitrile (0–95% over 60 min) at 300 nL/min. Mass spectrometric parameters included a capillary temperature of 200 °C, ion spray voltage of 1800 V, and higher-energy collisional dissociation (HCD) fragmentation. Label-free quantification was performed via MaxQuant 1.3.0.5, with protein abundances normalized to spectral counts derived from the *Rhodococcus* sp. 21391 genome. Proteins with ≥ twofold differential expression ($P < 0.05$) across three technical replicates were considered significant.

Protein expression and purification

The genes encoding RsNpcA and RsNpcB were cloned into the vector pET22b(+) (Novagen, Madison, WI, USA) between the *Nde*I and *Xho*I restriction sites for recombinant proteins production in *Escherichia coli* strain BL21 (DE3) (Novagen). Recombinant bacterial cells were

grown in Luria Broth medium supplemented with 50 μg/mL ampicillin at 37 °C to an OD600 of 0.6. By the addition of 0.5 mM isopropyl-β-D-1-thiogalactopyranoside and lowering the temperature to 16 °C, protein expression was induced. After 16 h-induction, cells were collected by centrifugation at 8000×*g* for 10 min. Harvested cells were resuspended in binding buffer (20 mM Tris–HCl, pH 8.0, 500 mM NaCl, and 5 mM imidazole) and lysed by sonication with 1-s pulse/1-s pause cycle for 15 min on ice. Cell debris was removed by centrifuging at 10,000×*g* for 30 min. The supernatant was applied to a Ni-nitrilotriacetic acid resin (Qiagen, Hilden, Germany), and washed with a washing buffer (20 mM Tris–HCl, pH 8.0, 500 mM NaCl, and 20 mM imidazole) to remove non-specifically bound proteins. The target protein was then eluted using an elution buffer (20 mM Tris–HCl, pH 8.0, 500 mM NaCl, and 200 mM imidazole). To further purify the protein, the eluate was applied to a Mono Q column (GE Healthcare, Chicago, IL, USA) and eluted using a linear gradient of NaCl ranging from 0 to 1.0 M. The purified protein was concentrated to 10 mg/mL using the Amicon Ultra-15 device (molecular weight cut-off = 10 kDa; Merck-Millipore Co., Burlington, MA, USA).

Enzyme assay

The reaction of the reductase component of PNP monooxygenase (RsNpcB) contained 200 μM nicotinamide adenine dinucleotide phosphate (NADPH), and 20 μM flavin adenine dinucleotide (FAD) in 50 mM Tris–HCl buffer (pH 7.5). Assays were initiated by the addition of 2.5 μg/mL purified RsNpcB. The activity was assayed at 25 °C by measuring the decrease in absorption of NADPH at 340 nm ($\varepsilon = 6220\ M^{-1}\ cm^{-1}$). The reaction of PNP monooxygenase contained 800 μM NADPH, 20 μM FAD, 50 mM Tris–HCl buffer (pH 7.5), 0.1 μg/mL purified RsNpcB, and 15 μg/mL purified RsNpcA. The reaction was initiated by the addition of 100 μM of the substrate PNP, and the enzyme activity was calculated by measuring the uptake of the substrate PNP at 405 nm ($\varepsilon = 18{,}000\ M^{-1}\ cm^{-1}$).

Site-directed mutagenesis

The desired mutants at the target sites were generated using a one-step targeted mutagenesis method [20]. Polymerase chain reaction amplification was performed using Phanta Master DNA polymerase (Vazyme, Nanjing, China) according to the following procedure: 95 °C for 10 min, followed by 30 cycles of 95 °C for 30 s, 50 °C for 30 s, and 72 °C for 4 min, and then 72 °C for 10 min. The harvested PCR products were digested with *Dpn*I (Vazyme) to remove the methylated parental plasmid and then purified using a PCR product purification kit (GenStar, Suzhou, China). Linearized plasmid derivatives were transferred into *E. coli* XL-10 cells. Plasmids from verified positive clones were extracted and retransferred into *E. coil* BL21 (DE3) cells for expression to generate mutant enzymes.

Crystallization, X-ray diffraction, and structure determination

Protein crystallization was carried out via the sitting drop method, mixing 0.4 μL of purified RsNpcA (8 mg/mL) with an equal volume of reservoir solution comprising 0.056 M NaH_2PO_4 and 1.344 M K_2HPO_4. The resulting mixture was equilibrated for 48 h at 20 °C in a 96-well protein crystallization plate (Violamo, Osaka, Japan). The obtained crystals were flash-frozen in a cryoprotectant that consisted of the reservoir solution supplemented with 22% ethylene glycol. The X-ray diffraction data were collected on the BL-5A beamline at the Photon Factory (Tsukuba, Japan), and were indexed, integrated, and scaled using the XDS software [21]. The structure of RsNpcA was elucidated using molecular replacement with Molrep of the CCP4 suite [22]. The search model used the automatic coordinates predicted by alphafold2. REFMAC [23], phenix.refine [24], and COOT [25] were used to perform iterative refinement cycles. Details regarding the data collection and the refinement statistics are shown in Table 2. All structural representations were generated using PyMOL (v.2.3; Schrödinger, LLC., New York, NY, USA). Atomic coordinates and structural factors for RsNpcA were deposited in the Protein Data Bank under accession number 9J9J.

Results

Efficient PNP metabolism by *Rhodococcus* sp. 21391

The isolated mangrove soil bacterium strain 21391 could utilize PNP as its sole carbon source for growth and reproduction in the MSM medium. It completely degraded 300 μM PNP within 18 h whilst simultaneously releasing an equivalent amount of nitrite ions without induction (Fig. 1a). During the utilization of PNP by strain 21391, the meso-hydroxylated intermediate *p*-nitrocatechol was observed (Fig. 1b). Complete degradation of PNP, up to 1300 μM, was achieved within 48 h, highlighting the high substrate concentration tolerance of the strain. At a substrate concentration of 1600 μM, the biodegradation efficiency decreased significantly, with a degradation rate of approximately 20% after 72 h (Fig. 1c). 16S rRNA sequencing analysis revealed that this strain belongs to the Actinobacteria phylum, specifically within the genus *Rhodococcus*, and shares up to 99% sequence identity with *Rhodococcus opacus* 1CP (Fig. 1d).

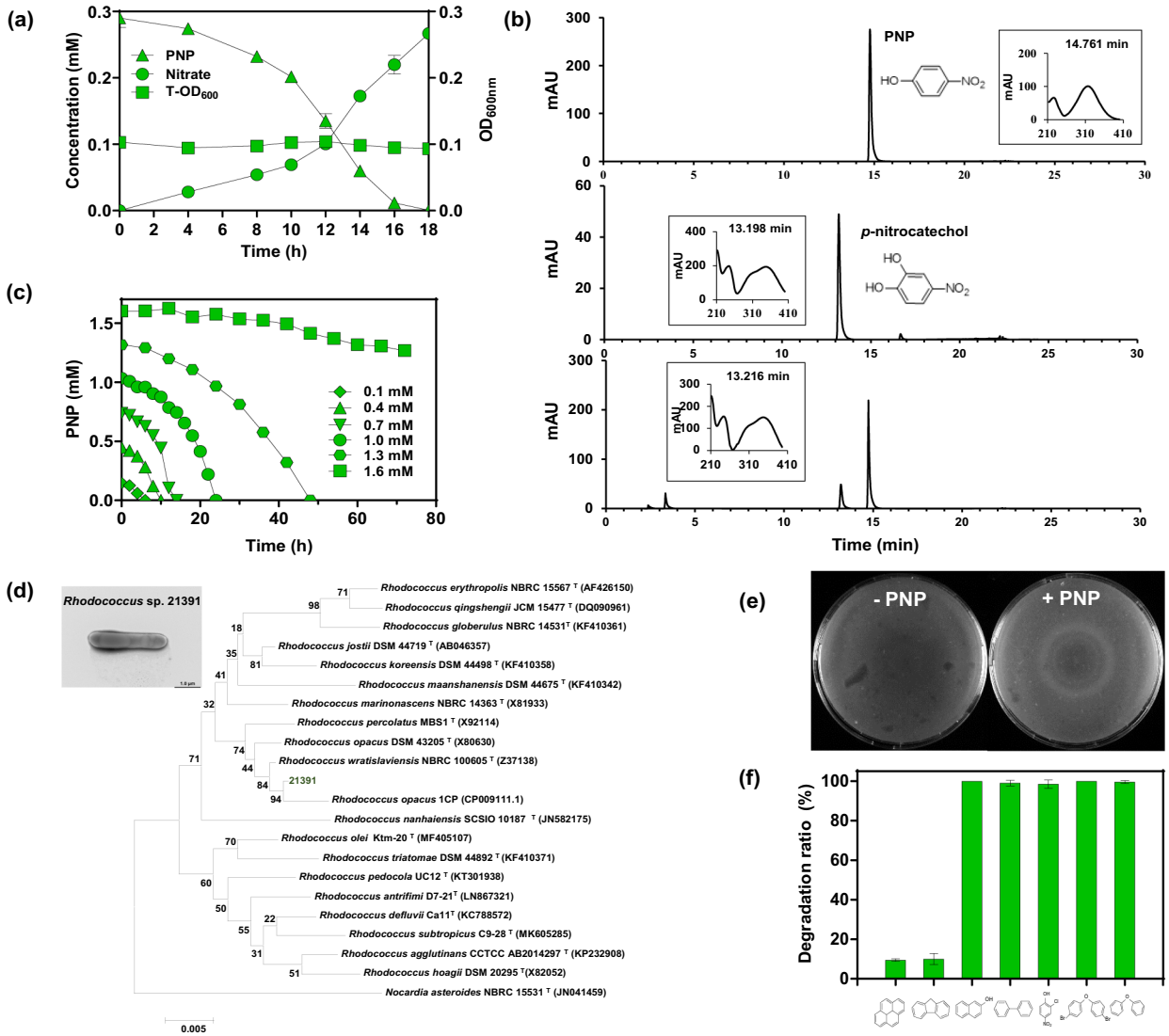

Fig. 1 Efficient biodegradation of PNP by strain *Rhodococcus* sp. 21391. **a** Degradation kinetics of 300 μM PNP by cells of strain 21391. The depletion of PNP (green triangle), cell density (OD600 of culture, green square), and nitrite released in the medium during the 18-h culture were monitored. **b** HPLC analysis of PNP catabolic intermediate by strain 21391. Comparison of retention times and spectra with standards of PNP (upper) and *p*-nitrocatecol (middle) show that *p*-nitrocatecol is an intermediate product of PNP degradation. **c** Effect of PNP concentrations (0.1–1.6 mM) on PNP biodegradation by strain 21391. **d** Neighbor-joining phylogenetic tree showing the evolutionary relationship between *Rhodococcus* sp. 21391 and other *Rhodococcus* spp. **e** Chemotaxis response of strain 21391 in the drop assay. PNP (1 μL) at a concentration of 1 mM was spotted onto the plate containing cells of strain 21391 and incubated for 24 h at 30 °C. The plates were prepared from MSM medium supplemented with 0.4% (*m/v*) agarose. The plate without PNP spotting was used as a negative control. **f** Degradation of different benzenes by strain 21391. Cells of strain 21391 were resuspended in MSM medium to OD600 = 0.1, while pyrene, fluorene, β-naphthol, biphenyl, 2-chloro-4-nitrophenol, dibromodiphenyl ether, and diphenyl ether were added to a final concentration of 300 μM. The content of residual benzenes was detected by HPLC after incubation for 72 h at 25 °C and 100 rpm shaking. Three replicates were set up for all the tests

In the drop assay, a pronounced chemotaxis of strain 21391 towards the PNP substrate (Fig. 1e) was observed. This chemotactic response likely assists the strain with efficient substrate recognition and utilization, despite the absence of flagella, a feature atypical of *Rhodococcus* [26]. Additionally, the strain exhibited the ability to effectively degrade several compounds other than PNP such as 2-chloro-4-nitrophenol, diphenyl ether, dibromodiphenyl ether, and β-naphthol (Fig. 1f), thereby indicating its considerable potential in benzene metabolism.

Identification of the PNP metabolism gene cluster

With a total genome length of 9.42 Mb, 21391 possesses one of the most expansive prokaryotic genomes [27]. It consists of a single circular chromosome and three plasmids (Fig. 2a). This genome encompasses a repertoire of 9055 proteins, including 76 genes dedicated to dioxygenases (54 of which are aromatic compound dioxygenases), 118 genes dedicated to monooxygenases (33 of which are aromatic compound monooxygenases), and 18 genes dedicated to dehydrogenases (nine of which are aromatic compound dehydrogenases). The majority of these functionally relevant protein-coding genes are densely clustered within the genome and orchestrate the metabolic pathways associated with benzene compounds. Thus, this analysis delineated 22 peripherally metabolized and eight centrally metabolized benzene degradation pathways (Table S1), which contain a comprehensive suite of genes putatively involved in the degradation metabolism of PNP (Fig. 2b). The presumed PNP-degrading gene cluster consists of four genes (*npc*A-D) encoding four enzymes (*p*-nitrophenol monooxygenase oxidizing component, flavin reductase, hydroxyquinol1,2-dioxygenase, and maleylacetate reductase) and one gene *pnp*R encoding a TetR transcriptional negative regulator protein.

Strain 21391 displayed inducibility for the degradation of PNP, and cells subjected to the PNP-inducible treatment showed increased degradation efficiency (Fig. 2c). To identify the key enzymes responsible for PNP degradation, the protein expression of strain 21391 with and without the supplementation of PNP was quantitatively investigated using label-free protein analysis, and significant changes in the protein expression profiles were observed (Table S2). In particular, the expression of the oxidizing component of *p*-nitrophenol monooxygenase, RsNpcA, was significantly up-regulated by 385-fold, and the *p*-nitrophenol monooxygenase reductase component, RsNpcB, switched from a state of non-expression to active expression. In addition, the hydroxyquinol 1,2-dioxygenase, RsNpcC, showed a staggering 499-fold up-regulation (Fig. 2d). These results strongly suggest the active involvement of the gene cluster in the degradation of PNP by strain 21391 and reveal the underlying biochemical mechanisms (Fig. 2b).

Biochemical characterization of the two-component PNP monooxygenase

The two-component monooxygenase RsNpcAB catalyzes the initial oxidative step in PNP metabolism, which is a key rate-limiting process in PNP degradation [28, 29]. To test their enzymatic properties, the recombinant enzymes RsNpcA and RsNpcB were produced using an *E. coli* expression system, purified in vitro, and characterized (Fig. 3a). The reducing component, RsNpcB, transfers electrons from nicotinamide to riboflavin, which then binds to the oxidase component RsNpcA to enable PNP hydroxylation. Despite their functional collaboration, size exclusion chromatography analysis revealed the absence of a complex formation in solution (Fig. 3b).

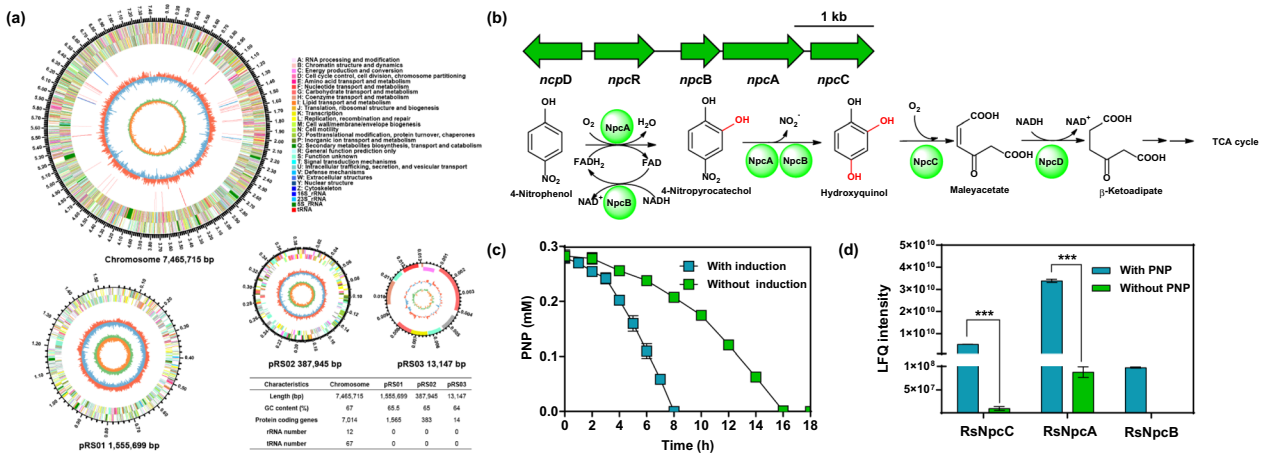

Fig. 2 Catabolic pathway of PNP deduced by genomic and proteomic analyses. **a** Complete genome, with one chromosome and three plasmids (pRS01, pRS02, and pRS03), of strain *Rhodococcus* sp. 21391. **b** PNP degradation gene cluster and its corresponding degradation pathways identified from the genomic sequence. The two-component *p*-nitrophenol monooxygenase catalyzes the formation of 1,2,4-benzenetriol from PNP, which in turn is oxidized and ring-opened by NpcC to enter the tricarboxylic acid cycle. **c** Comparison of PNP degradation efficiency of PNP by strain 21391 cells with and without induction. After PNP induction, the ability of strain 21391 to metabolize PNP is significantly enhanced, and complete degradation of 300 μM PNP is achieved within 8 h. **d** Comparison of the expression level of PNP pathway enzymes in strain 21391 in the presence and absence of PNP

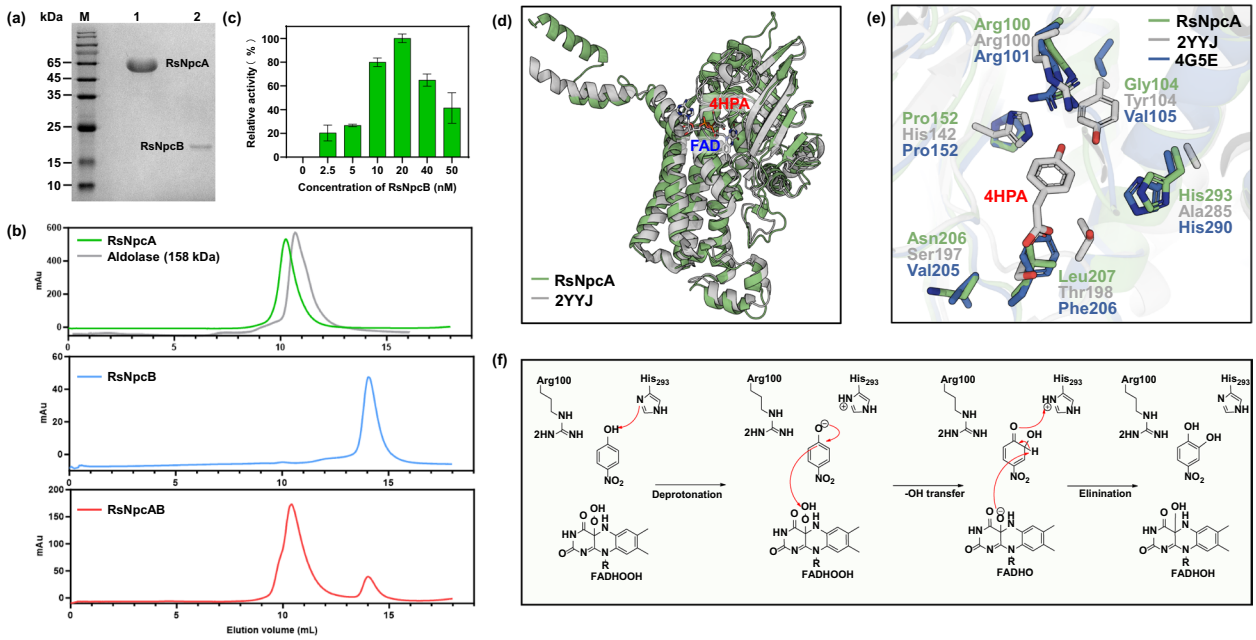

Fig. 3 Biochemical and structural analysis of two-component *p*-nitrophenol monooxygenase RsNcpAB from *Rhodococcus* sp. 21391. **a** Sodium dodecyl-sulfate polyacrylamide gel electrophoresis analysis of the two components of *p*-nitrophenol monooxygenase, RsNcpA and RsNcpB. Lane M, protein molecular weight marker. Lane 1, purity of the oxidative component RsNcpA. Lane 2, purity of the oxidative component RsNcpB. **b** Size-exclusion chromatography of the two-component *p*-nitrophenol oxygenase using Superdex 200 increase 10/300 GL column. Oligomeric analysis of purified RsNcpA (upper), RsNcpB (middle), and their equimolar mixture (lower) revealed no significant binding between the two components. **c** Effect of different ratios of A and B proteins on enzyme activity. The final concentration of RsNpcA in the reaction solution was kept at 1 μM, and the enzyme activity was examined with different amounts of RsNpcB. **d** Overlay of crystal structures of RsNcpA and ligand-bound HpaB (PDB entry: 2YYJ) reveal putative substrate binding sites. **e** Close-up view of the substrate binding sites. The superimposition of the binding sites of RsNcpA, HpaB, and TftD (PDB entry: 4G5E). **f** Proposed catalytic mechanism of RsNcpA based on the structural and biochemical analyses. The residue His1293 abstracts a proton from the hydroxyl group of PNP, and a hydroxyl group of the C4a-hydroperoxyflavin intermediate is introduced to the ortho position on the aromatic ring by electrophilic attack. The dienone form of the product is finally rearomatized to *p*-nitrocatechol, and C4a-hydroxyflavin is formed

Kinetic assays revealed RsNpcB accepts both NADH and NADPH as electron donors and uses FAD or FMN as electron acceptors. While FAD and FMN supported comparable catalytic efficiencies (Table 1), NADPH yielded a twofold higher turnover rate than NADH. Optimal activity required a 50:1 molar ratio of RsNpcA to RsNpcB (Fig. 3c), consistent with the stoichiometry observed in other two-component systems [14]. RsNpcA displayed maximal activity at 25 °C and pH 7.5, and its substrate spectrum included halogenated phenols (Table 2). Although PNP was the preferred substrate ($k_{cat}/K_m = 14\,15.68 \pm 56.07$ M^{-1} s^{-1}), RsNpcA also oxidized 2-chloro-4-nitrophenol, *p*-fluorophenol, and *p*-bromophenol, with the lowest efficiency toward *p*-iodophenol ($k_{cat}/K_m = 23.57 \pm 1.92$ M^{-1} s^{-1}).

While RsNpcAB's PNP affinity matches that of *Burkholderia* sp. SJ98 [30] and *Pseudomonas* sp. WBC-3 [31] enzymes, its lower catalytic efficiency explains strain 21391's slower PNP metabolism. Critically, this study identifies RsNpcAB as the first reported two-component monooxygenase capable of degrading halogenated phenols. This unprecedented substrate promiscuity expands its biotechnological potential for detoxifying halogenated pollutants, a capability lacking in previously characterized PNP-degrading systems.

Table 1 Kinetic parameters of RsNpcB

Substrate	K_m (μM)	k_{cat} (s^{-1})	$k_{cat}/K_m \times 10^6$ (M^{-1} s^{-1})
NADH[a] + FAD	0.11 ± 0.02	4.36 ± 1.4	40.20 ± 3.8
NADH[a] + FMN	0.02 ± 0.007	1.08 ± 0.094	49.63 ± 1.007
NADH + FAD[b]	45.47 ± 10.78	2.60 ± 1.03	0.058 ± 0.004
NADPH + FAD[b]	16.44 ± 4.62	1.83 ± 0.67	0.12 ± 0.008

Enzymatic analyses of RsNpcB were conducted in 50 mM Tris–HCl buffer (pH 7.5) at 25 °C

NADH dihydronicotinamide adenine dinucleotide, *NADPH* dihydronicotinamide-adenine dinucleotide phosphate, *FAD* flavin adenine dinucleotide, *FMN* flavin mononucleotide

[a] Concentration of NADH in the reaction was kept constant at 200 μM with FAD or FMN varying from 0.2–1.0 μM

[b] Concentration of FAD in the reaction was kept constant at 20 μM with NADH or NADPH varying from 20–220 μM

Table 2 Kinetic parameters of RsNpcA towards various nitrophenols

Substrate	K_m (μM)	k_{cat} (min^{-1})	k_{cat}/K_m (M^{-1} s^{-1})	
PNP	56.70 ± 9.60	4.74 ± 0.60	1415.68 ± 56.07	This study
2NP	N.D	N.D	N.D	
2C4NP	21.94 ± 3.34	1.62 ± 0.10	1231.79 ± 116.25	
4FP	630.42 ± 118.90	1.98 ± 0.36	52.3 ± 0.30	
4CP	31.41 ± 0.64	0.66 ± 0.01	343.72 ± 13.53	
4BP	15.57 ± 0.83	0.60 ± 0.01	642.75 ± 28.25	
4IP	208.53 ± 39.33	0.294 ± 0.03	23.57 ± 1.92	
PNP	25.4 ± 3.63	–	–	Ref. [30]
PNP	20.3 ± 2.70	–	11,083.33 ± 716.66	Ref. [31]

Enzyme assay was carried out in 50 mM Tris–HCl buffer (pH 7.5) at 25 °C, with 800 μM NADH and 20 μM FAD

PNP p-nitrophenol, *2NP o*-nitrophenol, *2C4NP* 2-chloro-4-nitrophenol, *4FP p*-fluorophenol, *4CP p*-chlorophenol, *4-BP p*-bromophenol, *4IP p*-iodophenol, *N.D.* no activity detected

Table 3 X-ray data collection and refinement statistics for the crystal structure of RsNpcA

Parameters	RsNpcA
Data collection	
Beamline	BL5A
Space group	I 41 2 2
Cell dimensions	
a, *b*, *c*, Å	149.561, 149.561, 322,141
Wavelength, Å	1.00000
Resolution, Å[a]	49.27–2.40 (2.45–2.40)
Total reflections	954,764
Unique reflections	71,504 (4527)
Redundancy	13.4 (13.7)
R_{sym} or R_{merge}[a,b]	0.077 (1.141)
I/σ	21.2 (2.6)
CC (1/2)	1.0 (0.923)
Completeness, %	99.8 (99.1)
Refinement	
R_{work}/R_{free}[c]	0.2399/0.2710
No. of protein atoms	11,806
Water	101
Average B factor, $Å^2$	58.65
Bond lenghth RMSZ, Å	0.436
Bond angles RMSZ, °	0.678
Ramachandran distribution	
Favored, %	96.93
Allowed, %	2.59
Outliers, %	0.48

[a] Numbers in parentheses represent the values for the highest-resolution shell

[b] $R_{sym} = \sum_{hkl}\sum_i |I_i - \langle I\rangle| / \sum_{hkl}\sum |\langle I\rangle|$, where I_i is the intensity for the *i*th measurement of an equivalent reflection with indices *h*, *k*, and *l*

[c] R_{free} calculated with 5% of the reflections set aside randomly throughout the refinement

Structural and molecular insights into the catalysis of RsNpcA

To gain insights into the substrate recognition and catalytic mechanism of *p*-nitrophenol monooxygenase, the crystal structure of RsNpcA at a resolution of 2.4 Å with a space group of *I*4122 was determined (Table 3). Three protein molecules were identified within the asymmetric unit, while size exclusion chromatography analysis suggested that RsNpcA exists in a homotetramer state in solution (Fig. 3b). The structure of RsNpcA consists of 12 β-folds and 20 α-helices, with a distinctive α-helix extension structure at the C-terminus characteristic of phenol monooxygenases [32, 33]. Despite efforts to incorporate FAD into the crystallization system for co-crystallization with RsNpcA, no FAD ligand was observed in the resolved protein structures. The absence of FAD in numerous crystal structures of two-component monooxygenases may be due to a transient binding of FAD to the enzyme or to the requirement for the enzyme to bind to the reduced FAD [33–35].

To delineate the active sites of RsNpcA, its structure was aligned with that of the oxidase component of 4-hydroxyphenylacetate 3-monooxygenase from *Thermus thermophilus* HB8 (PDB entry: 2YYJ), which binds FAD and 4-hydroxyphenylacetate (Fig. 3c). The comparative analysis identified potential substrate-interacting residues in RsNpcA, in particular Arg100, Pro152, Leu207, and His293 (Fig. 3d). However, these residues exhibited low conservation, in particular, Pro152 in RsNpcA replaces His142, a crucial general base in 4-hydroxyphenylacetate 3-monooxygenase for proton abstraction from the substrate. Similarly, in 2,4,5-TCP 4-monooxygenase from *Cupriavidus necator* JMP134, the corresponding residue is proline, implying an alternative residue His289 (His293 in RsNpcA) as a general base [36]. When His293 of RsNpcA was mutated to alanine ($RsNpcA^{H293A}$), the enzyme retained PNP catalytic activity, albeit with a 58-fold decrease in efficiency (Table 4), suggesting an essential role in catalysis. In addition, mutagenesis of the conserved residue Arg100 to alanine ($RsNpcA^{R100A}$) resulted in a complete loss of catalytic function, underscoring the pivotal role of Arg100 in enzymatic activity.

Discussion

The newly isolated mangrove bacterium *Rhodococcus* sp. 21391 efficiently mineralizes p-nitrophenol (PNP) as its sole carbon source, degrading 300 μM PNP within 8 h under induction (Fig. 2c). This performance surpasses previously characterized strains, including *R. wratislaviensis* [37] and *R. imtechensis* RKJ300 [38], which required 34 h and 12 h to degrade 50 mg/L (36 μM) and

Table 4 Kinetic parameters of RsNpcA and its mutants

Enzyme	K_m (μM)	k_{cat} (min^{-1})	k_{cat}/K_m (M^{-1} s^{-1})
RsNpcA	56.70 ± 9.60	4.74 ± 0.60	1415.68 ± 56.07
RsNpcA^{H293A}	52.65 ± 3.72	0.06 ± 0.005	28.44 ± 0.13
RsNpcA^{R100A}	N.D	N.D	N.D

N.D. no activity detected

300 μM PNP, respectively. Strain 21391 also demonstrates broad metabolic versatility, degrading diverse benzenering pollutants (Fig. 1f). This functional breadth may arise from its chemotactic response to aromatic compounds (Fig. 1e) and a robust intracellular enzyme repertoire, including the two-component monooxygenase RsNpcAB identified in this study. Notably, strain 21391 tolerates PNP concentrations exceeding 1 mM (Fig. 1c), a trait rare among reported degraders. Collectively, these properties position *Rhodococcus* sp. 21391 as a promising candidate for bioremediation of phenolic-contaminated industrial wastewater, where its high substrate tolerance and broad metabolic capacity could address recalcitrant pollutants.

Chemotaxis mediates bacterial interactions with environmental chemicals and plays a key role in the recognition of chemicals utilized by bacteria for "feeding" [39, 40]. Of note, while members of *Rhodococcus* lack flagella and are generally considered to be non-motile [26], strain 21391 sensed the substrate PNP and exhibited chemotaxis in the present study. This is not the first report of the chemotactic motility of *Rhodococcus*, for example, *R. erythropolis* U23A showed chemosensitizing effects on Arabidopsis root leachate [41]; the cell density of the plant roots was tenfold higher than that of the surrounding sandy soil. In addition, biphenyl and benzoic acid chemotaxis has also been observed in *R. ruber* SS1 and *R. pyridinivorans* SS2 [42]. The present study identified genes associated with bacterial gliding and twitching motility in the genome of strain 21391 (Table S3). The mechanism by which these genes mediate chemotaxis warrants further in-depth study.

Based on genomic and proteomic analyses, the gene cluster involved in PNP metabolism in strain 21391 was identified, and the structure and catalytic properties of the key enzymes were characterized, thus elucidating the mechanism of PNP metabolism in this bacterium at the molecular level. In particular, RsNpcAB, the two-component *p*-nitrophenol monooxygenase derived from strain 21391, was found to have a broad substrate spectrum, and not only catalyzes the efficient oxidation of nitrophenols (including PNP and 2-chloro-4-nitrophenol), but can also utilize a wide range of para-halogenated phenols as substrates (Table 2). These results suggest that the enzyme is likely to have potential for development in the field of biocatalysis. Since the substrate binding site of RsNpcA consists of several residues including small spatially hindering residues such as Gly104, Pro152, and Leu207 (Fig. 3e), it is hypothesized that the broad substrate selectivity of *p*-nitrophenol monooxygenase is likely because the enzyme has a large substrate pocket that can accommodate the binding of multiple substrate molecules. In addition, based on the crystal structure and site mutation analysis, it is evident that residues Arg100 and His293 in the active center of RsNpcA play an essential role in catalysis. Therefore, based on previous research [36], a catalytic pathway in which residue His293 is directly involved in catalysis as a general base, and Arg100 provides the appropriate ionized environment to support the reaction, is proposed (Fig. 3f).

Conclusions

This study isolated a new mangrove soil bacterium strain, *Rhodococcus* sp. 21391 that can efficiently metabolize PNP. The strain completely degraded 300 μM PNP within 8 h and possessed the ability to degrade a variety of benzene compounds, demonstrating its metabolic potential and applicability in the field of environmental remediation. Using genomic and comparative proteomic analysis, the gene cluster responsible for PNP metabolism in *Rhodococcus* sp. 21391 was identified, and a key two-component *p*-nitrophenol oxidase (RsNpcAB) with a uniquely broad substrate profile was discovered. Considering the potential application of RsNpcAB in the transformation of environmental organic pollutants, the crystal structure of the oxidizing component of *p*-nitrophenol oxidase, RsNpcA, was revealed. Based on structural and point mutation analyses, a model of the enzyme's catalytic mechanism was proposed, providing fundamental support for the further exploitation of this enzyme. This study constitutes a useful microbial resource for the bioremediation of environmental benzene organic pollutants represented by PNP. The revealed metabolic mechanism and key enzymes provide a solid foundation for further development of more efficient environmental remediation.

Supplementary Information

The online version contains supplementary material available at https://doi.org/10.1186/s12934-025-02712-1.

Supplementary Material 1.

Acknowledgements
This work was supported by National Natural Science Foundation of China (U23A2036), Guangdong Basic and Applied Basic Research Foundation (2025A1515010929, 2023A1515110329), and Guangzhou Science and Technology Project (2023A04J0901).

Author contributions
Jian Yang: writing—original draft, visualization, resources, validation, supervision, conceptualization. Shanshan Lin: writing—review & editing, methodology, investigation, data curation. Wei Li: writing—review & editing, validation. Xianjie Wang: writing—review & editing, validation. Zhangliang Wei: writing—review & editing, validation. Ru Li: writing—review & editing, methodology, investigation, data curation, funding acquisition.

Funding
This study was funded by National Natural Science Foundation of China (U23A2036); Guangdong Basic and Applied Basic Research Foundation (2023A1515110329); Guangzhou Science and Technology Project (2023A04J0901).

Availability of data and materials
No datasets were generated or analysed during the current study.

Declarations

Competing interests
The authors declare no competing interests.

Author details
[1]School of Life and Health Technology, Dongguan University of Technology, Dongguan, China. [2]CAS Key Laboratory of Tropical Marine Bio-resources and Ecology, South China Sea Institute of Oceanology, Guangzhou, China. [3]University of the Chinese Academy of Sciences, Beijing, China.

Received: 22 January 2025 Accepted: 3 April 2025
Published online: 17 April 2025

References

1. Arora PK, Srivastava A, Singh VP. Bacterial degradation of nitrophenols and their derivatives. J Hazard Mater. 2014;266:42–59.
2. Rubio MA, Lissi E, Herrera N, Perez V, Fuentes N. Phenol and nitrophenols in the air and dew waters of Santiago de Chile. Chemosphere. 2012;86:1035–9.
3. Zhang Z, Xi H, Yu Y, Wu C, Yang Y, Guo Z, Zhou Y. Coupling of membrane-based bubbleless micro-aeration for 2,4-dinitrophenol degradation in a hydrolysis acidification reactor. Water Res. 2022;212: 118119.
4. Eichenbaum G, Johnson M, Kirkland D, O'Neill P, Stellar S, Bielawne J, DeWire R, Areia D, Bryant S, Weiner S, et al. Assessment of the genotoxic and carcinogenic risks of p-nitrophenol when it is present as an impurity in a drug product. Regul Toxicol Pharmacol. 2009;55:33–42.
5. Fernandes Silva E, Varela ASJ, Cardoso TF, Stefanello FM, Kalb AC, Martinez PE, Corcini CD. Reproductive toxicology of 2,4 dinitrophenol in boar sperm. Toxicol In Vitro. 2016;35:31–5.
6. Xue GH, Gao ML, Gu Z, Luo ZX, Hu ZC. The removal of *p*-nitrophenol from aqueous solutions by adsorption using Gemini surfactants modified montmorillonites. Chem Eng J. 2013;218:223–31.
7. Liu LQ, Deng GZ, Shi XY. Adsorption characteristics and mechanism of *p*-nitrophenol by pine sawdust biochar samples produced at different pyrolysis temperatures. Sci Rep. 2020;10:5149.
8. Gimeno O, Carbajo M, Beltran FJ, Rivas FJ. Phenol and substituted phenols AOPs remediation. J Hazard Mater. 2005;119:99–108.
9. Mehrizad A, Zare K, Aghaie H, Dastmalchi S. Removal of 4-chloro-2-nitrophenol occurring in drug and pesticide waste by adsorption onto nano-titanium dioxide. Int J Environ Sci Technol. 2012;9:355–60.
10. Shen W, Liu W, Zhang J, Tao J, Deng H, Cao H, Cui Z. Cloning and characterization of a gene cluster involved in the catabolism of *p*-nitrophenol from *Pseudomonas putida* DLL-E4. Bioresour Technol. 2010;101:7516–22.
11. Kitagawa W, Kimura N, Kamagata Y. A novel p-nitrophenol degradation gene cluster from a gram-positive bacterium, *Rhodococcus opacus* SAO101. J Bacteriol. 2004;186:4894–902.
12. Zhang SY, Sun W, Xu L, Zheng XM, Chu XY, Tian J, Wu NF, Fan YL. Identification of the p-nitrophenol catabolic pathway, and characterization of three enzymes involved in the hydroquinone pathway, in *Pseudomonas* sp. 1–7. BMC Microbiol. 2012;12:27.
13. Huo K, Liu Y, Huang R, Zhang Y, Liu H, Che Y, Yang C. Development of a novel promoter engineering-based strategy for creating an efficient para-nitrophenol-mineralizing bacterium. J Hazard Mater. 2022;424: 127672.
14. Min J, Zhang JJ, Zhou NY. A two-component para-nitrophenol monooxygenase initiates a novel 2-chloro-4-nitrophenol catabolism pathway in *Rhodococcus imtechensis* RKJ300. Appl Environ Microbiol. 2016;82:714–23.
15. Ren L, Jia Y, Zhang R, Lin Z, Zhen Z, Hu H, Yan Y. Insight into metabolic versatility of an aromatic compounds-degrading *Arthrobacter* sp. YC-RL1. Front Microbiol. 2018;9:2438.
16. Takeda H, Shimodaira J, Yukawa K, Hara N, Kasai D, Miyauchi K, Masai E, Fukuda M. Dual two-component regulatory systems are involved in aromatic compound degradation in a polychlorinated-biphenyl degrader, *Rhodococcus jostii* RHA1. J Bacteriol. 2010;192:4741–51.
17. Alam SA, Saha P. Evidence of *p*-nitrophenol biodegradation and study of genomic attributes from a newly isolated aquatic bacterium strain PNPG3. Soil Sediment Contam. 2023;32:994–1011.
18. Kumar S, Stecher G, Tamura K. MEGA7: molecular evolutionary genetics analysis Version 7.0 for bigger datasets. Mol Biol Evol. 2016;33:1870–4.
19. Kielkopf CL, Bauer W, Urbatsch IL. Bradford assay for determining protein concentration. Cold Spring Harb Protoc. 2020;2020: 102269.
20. Zheng L, Baumann U, Reymond JL. An efficient one-step site-directed and site-saturation mutagenesis protocol. Nucleic Acids Res. 2004;32: e115.
21. Kabsch W. Integration, scaling, space-group assignment and post-refinement. Acta Crystallogr D Biol Crystallogr. 2010;66:133–44.
22. Vagin A, Teplyakov A. Molecular replacement with MOLREP. Acta Crystallogr D Biol Crystallogr. 2010;66:22–5.
23. Murshudov GN, Skubak P, Lebedev AA, Pannu NS, Steiner RA, Nicholls RA, Winn MD, Long F, Vagin AA. REFMAC5 for the refinement of macromolecular crystal structures. Acta Crystallogr D Biol Crystallogr. 2011;67:355–67.
24. Adams PD, Afonine PV, Bunkoczi G, Chen VB, Davis IW, Echols N, Headd JJ, Hung LW, Kapral GJ, Grosse-Kunstleve RW, et al. PHENIX: a comprehensive Python-based system for macromolecular structure solution. Acta Crystallogr D Biol Crystallogr. 2010;66:213–21.
25. Emsley P, Cowtan K. Coot: model-building tools for molecular graphics. Acta Crystallogr D Biol Crystallogr. 2004;60:2126–32.
26. Majidzadeh M, Fatahi-Bafghi M. Current taxonomy of species and their role in infections. Eur J Clin Microbiol Infect Dis. 2018;37:2045–62.
27. McLeod MP, Warren RL, Hsiao WWL, Araki N, Myhre M, Fernandes C, Miyazawa D, Wong W, Lillquist AL, Wang D, et al. The complete genome of *Rhodococcus* sp. RHA1 provides insights into a catabolic powerhouse. Proc Natl Acad Sci USA. 2006;103:15582–7.
28. Kadiyala V, Spain JC. A two-component monooxygenase catalyzes both the hydroxylation of *p*-nitrophenol and the oxidative release of nitrite from 4-nitrocatechol in *Bacillus sphaericus* JS905. Appl Environ Microbiol. 1998;64:2479–84.
29. Takeo M, Yasukawa T, Abe Y, Niihara S, Maeda Y, Negoro S. Cloning and characterization of a 4-nitrophenol hydroxylase gene cluster from *Rhodococcus* sp. PN1. J Biosci Bioeng. 2003;95:139–45.
30. Min J, Zhang JJ, Zhou NY. The gene cluster for para-nitrophenol catabolism is responsible for 2-chloro-4-nitrophenol degradation in *Burkholderia* sp. strain SJ98. Appl Environ Microbiol. 2014;80:6212–22.
31. Zhang JJ, Liu H, Xiao Y, Zhang XE, Zhou NY. Identification and characterization of catabolic para-nitrophenol 4-monooxygenase and para-benzoquinone reductase from *Pseudomonas* sp. strain WBC-3. J Bacteriol. 2009;191:2703–10.
32. Shen X, Zhou D, Lin Y, Wang J, Gao S, Kandavelu P, Zhang H, Zhang R, Wang BC, Rose J, et al. Structural insights into catalytic versatility of the flavin-dependent hydroxylase (HpaB) from *Escherichia coli*. Sci Rep. 2019;9:7087.
33. Chenprakhon P, Wongnate T, Chaiyen P. Monooxygenation of aromatic compounds by flavin-dependent monooxygenases. Protein Sci. 2019;28:8–29.

34. Chang CY, Lohman JR, Cao H, Tan K, Rudolf JD, Ma M, Xu W, Bingman CA, Yennamalli RM, Bigelow L, et al. Crystal structures of SgcE6 and SgcC, the two-component monooxygenase that catalyzes hydroxylation of a carrier protein-tethered substrate during the biosynthesis of the enediyne antitumor antibiotic C-1027 in *Streptomyces globisporus*. Biochemistry. 2016;55:5142–54.
35. Guo Y, Li DF, Zheng J, Xu Y, Zhou NY. Single-component and two-component para-nitrophenol monooxygenases: structural basis for their catalytic difference. Appl Environ Microbiol. 2021;87: e0117121.
36. Hayes RP, Webb BN, Subramanian AK, Nissen M, Popchock A, Xun L, Kang C. Structural and catalytic differences between two FADH(2)-dependent monooxygenases: 2,4,5-TCP 4-monooxygenase (TftD) from *Burkholderia cepacia* AC1100 and 2,4,6-TCP 4-monooxygenase (TcpA) from *Cupriavidus necator* JMP134. Int J Mol Sci. 2012;13:9769–84.
37. Gemini VL, Gallego A, de Oliveira VM, Gomez CE, Manfio GP, Korol SE. Biodegradation and detoxification of *p*-nitrophenol by. Int Biodeterior Biodegrad. 2005;55:103–8.
38. Ghosh A, Khurana M, Chauhan A, Takeo M, Chakraborti AK, Jain RK. Degradation of 4-nitrophenol, 2-chloro-4-nitrophenol, and 2,4-dinitrophenol by *Rhodococcus imtechensis* strain RKJ300. Environ Sci Technol. 2010;44:1069–77.
39. Keegstra JM, Carrara F, Stocker R. The ecological roles of bacterial chemotaxis. Nat Rev Microbiol. 2022;20:491–504.
40. Celani A, Vergassola M. Bacterial strategies for chemotaxis response. Proc Natl Acad Sci USA. 2010;107:1391–6.
41. Toussaint JP, Pham TT, Barriault D, Sylvestre M. Plant exudates promote PCB degradation by a rhodococcal rhizobacteria. Appl Microbiol Biotechnol. 2012;95:1589–603.
42. Wang H, Hu JX, Xu K, Tang XJ, Xu XH, Shen CF. Biodegradation and chemotaxis of polychlorinated biphenyls, biphenyls, and their metabolites by *Rhodococcus* spp. Biodegradation. 2018;29:1–10.

Publisher's Note